Production of oil-in-water emulsions with varying dispersed-phase content using confined impinging jet mixers

Tripodi, Ernesto; Lazidis, Aris; Norton, Ian; Spyropoulos, Fotios

DOI:
10.1021/acs.iecr.9b00634

Document Version
Publisher's PDF, also known as Version of record

Citation for published version (Harvard):
Tripodi, E, Lazidis, A, Norton, I & Spyropoulos, F 2019, 'Production of oil-in-water emulsions with varying dispersed-phase content using confined impinging jet mixers', *Industrial & Engineering Chemistry Research*, vol. 58, no. 32, pp. 14859-14872. https://doi.org/10.1021/acs.iecr.9b00634

I&EC research
Industrial & Engineering Chemistry Research

Article

Cite This: Ind. Eng. Chem. Res. 2019, 58, 14859−14872

pubs.acs.org/IECR

Production of Oil-in-Water Emulsions with Varying Dispersed-Phase Content using Confined Impinging Jet Mixers

Ernesto Tripodi,* Aristodimos Lazidis, Ian T. Norton, and Fotis Spyropoulos

School of Chemical Engineering, University of Birmingham, B15 2TT Birmingham, United Kingdom

Supporting Information

ABSTRACT: This work reports for the first time on the use of Confined Impinging Jet Mixers (CIJM) for the production of emulsions with dispersed-phase content up to 80 wt %, in both the surfactant-poor and -rich regimes, following the exposure to varying CIJM hydrodynamic conditions. It was observed computationally and experimentally that the CIJM capacity resulted strictly dependent on the mass jet flow rate (W_{jet} > 176 g/min) and the pre-emulsion droplet size (>10 μm). CIJM emulsification performance remained (almost) unaffected by the variation in the oil mass fraction. All systems showed the lowest droplet size (∼8 μm) and similar droplet size distributions under the highest W_{jet}. Conditionally onto the Tween20 availability, the emulsion $d_{3,2}$ was primarily determined by formulation characteristics in the surfactant poor-regime and by the CIJM energy dissipation rate in the surfactant-rich regime. In conclusion, this study offers further insights into the CIJM suitability as a realistic alternative to already-established emulsification methods.

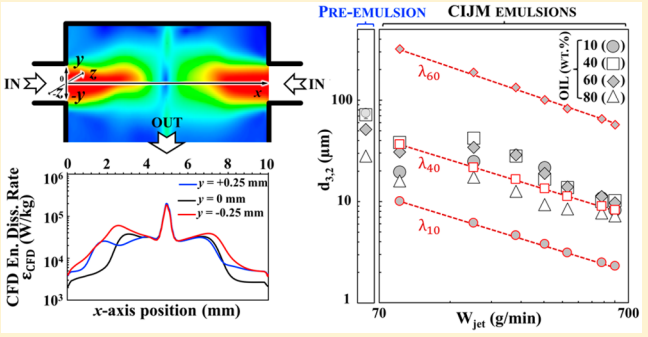

1. INTRODUCTION

In industrial practice, emulsification processing is commonly conducted within the turbulent regime caused by mixing (high-shear mixing, colloidal milling), pressure (high-pressure homogenization, microfluidisation), or ultrasound (sonication). The industrial appeal of these methods mainly stems from their capacity to allow continuous and large-throughput processing as well as their flexibility in terms of handling a wide range of materials.[1]

It is presently well-accepted that eddy formation plays a key part in droplet breakup under turbulence, with the smallest eddies determining the size of the smallest droplets achievable during emulsification.[2] According to the Kolmogorov-Hinze theory,[3,4] the size of these eddies is given by

$$\lambda_k = \bar{\varepsilon}^{-1/4} \rho_c^{-3/4} \eta c_c^{3/4} \quad (1)$$

where λ_k is the Kolmogorov eddy size, $\bar{\varepsilon}$ is the mean energy dissipation rate, and ρ_c and η_c are the density and viscosity of the continuous phase, respectively. Eq 1 holds for relatively dilute emulsions (oil fractions, ϕ < 40%), while for more concentrated systems (40% < ϕ < 75%), where viscosity may significantly deviate from that of the continuous phase, the η_c term is replaced by the emulsion viscosity (η_{em}).[5] Turbulent emulsification can normally occur in the turbulent inertial (TI) or turbulent viscous (TV) regimes.[5] In the TI regime, droplets deform under the action of hydrodynamic velocity and pressure fluctuations, resulting in droplets that tend to be larger than λ_k. In the TV regime, droplets deform under the action of viscous stresses both inside and between eddies; hence, their final size can be smaller than λ_k. Depending on the flow regime, the maximum stable droplet diameter (d_{max}),[6] which is defined as the largest droplet diameter that can resist droplet breakup, can be estimated from

$$d_{max}^{TI} = \bar{\varepsilon}^{-2/5} \rho_c^{-3/5} \gamma^{3/5} \quad (2)$$

$$d_{max}^{TV} = \bar{\varepsilon}^{-1/2} \eta_c^{-1/2} \rho_c^{-1/2} \gamma \quad (3)$$

where γ is the equilibrium interfacial tension.

Besides the hydrodynamic conditions established during emulsification, the final emulsion microstructure (in terms of the average droplet diameter and size distribution) will be also strongly influenced by the presence of surfactants.[7] Such surface-active species will tend to quickly adsorb at the oil/water interface, thus lowering the interfacial tension and facilitating droplet breakup, while at the same time (postadsorption) can assist in hindering coalescence phenomena associated with droplet contacts/collisions. Depending on the extremities of surfactant availability in the system, emulsification can take place under a surfactant-poor or a surfactant-rich regime.[8] On the one hand, in the surfactant-poor regime, although turbulence will promote droplet breakup, the resulting, more often partially covered, droplets will tend to merge. On the other hand, the surplus of surface-active species in the surfactant-rich regime ensures high adsorption rates and rapid interfacial stabilization,

Received: January 31, 2019
Revised: July 2, 2019
Accepted: July 8, 2019
Published: July 8, 2019

and thus final droplet size is heavily dependent on droplet disruption due to turbulence.

Despite their widespread industrial utilization and large product throughput capability, turbulent emulsification methods are still based on high-energy processing, and, as such, they are characterized by inherently low-energy efficiencies.[9] In addition, the energy dissipation distribution can be highly nonuniform, very often resulting in larger droplet sizes and/or broader droplet size distributions.[10] Such microstructural inconsistences can be partially addressed by repeatedly exposing the system to the original or similar turbulent processing conditions (multipassing). However, this also results in significant increases in the total energy input and further unavoidable reductions to the overall energy efficiency.

To mitigate these limitations, a number of studies have proposed alternative emulsification approaches, such as membrane or microchannel emulsification, where droplet formation occurs spontaneously rather than as a consequence of turbulence effects.[11,12] Though promising in terms of their much lower energy input and enhanced energy efficiency, these techniques are, at present, limited to bench-scale operation and are faced with a number of challenges to their industrial adoption, including their current incapacity to deliver high product throughputs.[13]

Emulsification using Confined Impinging Jet Mixers (CIJM) has more recently attracted some attention due to its potential to deliver both large throughputs combined to superior energy efficiencies.[14] Under CIJM operation, two jets (either of the two immiscible phases or of the same coarse pre-emulsion) collide at high velocities within a mixing cavity resulting in large energy dissipation rates. On the one hand, because of the small volume of the mixing chamber, the vast majority of the droplets is exposed to the high-energy dissipation zone, which allows great control over the final emulsion microstructure. On the other hand, the short residence time ($\sim 1 \times 10^{-3}$ s) within the mixing environment limits droplet collisions and thus coalescence phenomena. The mean energy dissipation rate ($\bar{\varepsilon}_{th}$) created following the jet collision can be theoretically estimated[15] according to

$$\bar{\varepsilon}_{th} = \frac{\Delta KE + 2Q_{jet}\Delta P}{\rho V_{CIJM}} \quad (4)$$

where ΔKE is the difference in kinetic energy between the two inlets and the outlet, Q_{jet} is the jet flow rate, ΔP is the pressure at which the jets collide, ρ represents the density of either the pure phase in each jet or of the pre-emulsion, and V_{CIJM} is the volume within the CIJM geometry where impingement takes place.

Originally, CIJM has been extensively studied from both an experimental and computational perspective for the production of nanoparticles due to the fast processing mixing times.[14] Transient Computational Fluid Dynamics (CFD) simulations on the CIJM have been used to find reliable scale-up criteria and describe mixing processes at the microscale.[16,17]

However, emulsification by using CIJM represents a relatively new topic; thus, the published literature in this area is somewhat limited. The emulsification performance of CIJM has been compared against that of established emulsification techniques, such as high-shear mixing, high-pressure homogenization, and sonication.[18] This work reported that, for significantly low energy inputs and at low oil volume fractions (5−10 vol %), CIJM produced smaller emulsion droplet sizes than both ultrasound treatment and high-shear mixing. Nevertheless, at energy inputs much higher than those achievable under CIJM operation, sonication and homogenization both generated emulsions of considerably smaller droplet sizes. In another study,[19] the production of dilute emulsions (5 and 10 vol %) as a function of jet flow rate (up to 610 g/min) and emulsifier type (Tween20, Span80, whey protein, lecithin, or sodium dodecyl sulfate, all at a fixed concentration of 1 wt %) was investigated. Within this range of hydrodynamic conditions, the smallest droplet sizes (~ 2 μm) were obtained at the highest jet flow rate (610 g/min) regardless of the type of emulsifier employed. Dilute emulsions of average droplet diameters below 700 nm were reported elsewhere,[20] but these could only be produced by coupling CIJM operation with sonication.

Clearly, although the appeal of the CIJM operation has indeed generated some knowledge regarding its processing performance in the field of emulsification, the level of understanding necessary to fully appreciate the method's true potential and possible industrial applicability is far from being achieved.

The aim of the present study is to extend current emulsification understanding associated with CIJM operation. This is obtained by investigating both computationally and experimentally the CIJM emulsification capacity followed by an experimental evaluation of the CIJM performance for the production of emulsions with a wide range of oil mass fractions, under either a surfactant-poor or a surfactant-rich regime, and as a result of exposure to varying CIJM hydrodynamic conditions and residence times. In all cases emulsions are produced by the CIJM treatment of coarse pre-emulsions, rather than the impingement of jets consisting of the two immiscible pure phases, and product microstructure is assessed in terms of final droplet size, droplet size distribution, and long-term stability (over a 40 d storage period).

The current work reports for the first time on the use of CIJM for the production of emulsions with dispersed-phase contents above 10 wt % (and up to 80 wt %) and relates the achieved microstructures to the hydrodynamic conditions (mean energy dissipation rate and jet mass flow rate) within the geometry, as characterized by both theoretical and computational models.

2. MATERIALS AND METHODS

2.1. Materials. All oil-in-water (o/w) emulsions were prepared by using as the continuous-phase deionized water obtained from a reverse osmosis filtration system. Commercial sunflower oil (viscosity = 50 mPa·s) purchased by a local retailer was used as the dispersed phase. Polysorbate20, that is, Tween20, (Hydrophilic−Lipophilic-Balance, HLB, = 16.7, molecular weight = 1227.54 g/mol) was supplied by Sigma-Aldrich Company and used as the emulsifier.

2.2. Emulsification Procedure. Emulsions were produced following a two-step procedure, which included (i) high-shear mixing to form the initial coarse pre-emulsion followed by (ii) emulsification within the CIJM.

2.2.1. Pre-Emulsion Preparation. For the preparation of the pre-emulsions, the required concentration of Tween20 was dissolved in water and mixed by using a magnetic stirrer for 10 min, before the addition of the desired amount of sunflower oil. Water, surfactant, and vegetable oil (together forming a solution of 500 mL) were then pre-emulsified by means of a Silverson L5 Series Laboratory High-Shear Mixer, equipped with an emulsor screen of 33 mm in diameter, for 3 min at defined rotational speeds. Details of the rotational speeds used for the preparation of the pre-emulsions are elucidated within the discussion of the Results section.

DOI: 10.1021/acs.iecr.9b00634
Ind. Eng. Chem. Res. 2019, 58, 14859−14872

2.2.2. Rheological Measurements. The flow behavior of all pre-emulsions was measured using a Kinexus Pro, stress-controlled rheometer (Malvern Instruments). Flow curves for the 10 and 40 wt % oil content pre-emulsions were obtained using a double gap geometry (with 2 mm gap thickness), while those for the 60 and 80 wt % systems were obtained using a cone and plate geometry (diameter: 40 mm; and angle: 4°). Each measurement was repeated three times. The average shear viscosity (η) values for the pre-emulsions of varying dispersed (oil) phase content are shown in Figure 1 as a function of the applied shear rate ($\dot{\gamma}$). All flow curves were fitted to a simple power-law model[21]

$$\eta = K \cdot \dot{\gamma}^{-1} \quad (5)$$

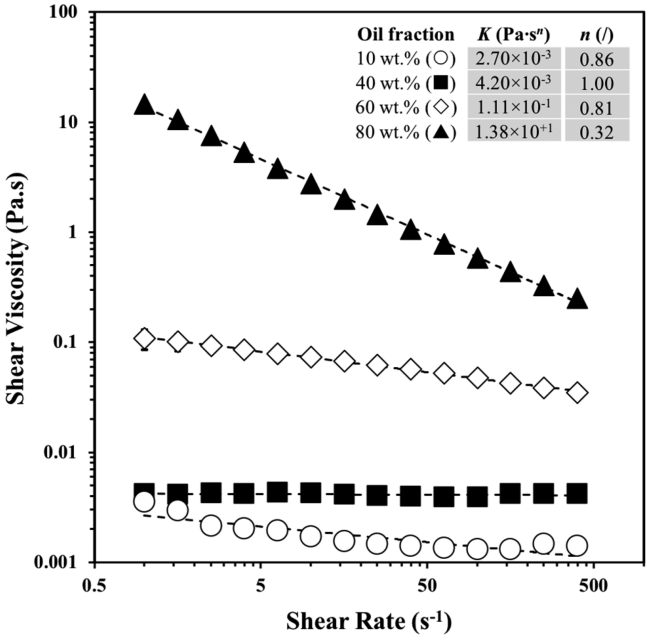

Figure 1. Flow curves for the 10 (○), 40 (■), 60 (◇), and 80 wt % (▲) oil content o/w pre-emulsions formed in the presence of 1 wt % Tween20. All shear viscosity data points are mean values (n = 3), and error bars represent one standard deviation of the mean; where not visible, error bars are smaller than the used symbols. Solid curves represent the best fit to a power-law model (see main text for detail). (inset) Consistency constant K and power-law index η parameters from the power-law model.

where K is the consistency constant, and η is the power-law index; the values of both are reported in the inset table of Figure 1.

2.2.3. Emulsion Preparation. In the second step, the pre-emulsions were processed through the CIJM geometry (Figure 2) by means of a single pulseless micropump (external gear pump) with jet mass flow rates varying from 85.2 to 702 g/min. Prior to impingement the flow was split into two equal streams by using a Y-junction, whereas after leaving the CIJM chamber emulsions samples were collected and stored in sample pots.

To study the effect of multipassing, emulsions were processed through the CIJM under fixed inlet mass jet flow rate (359 g/min) and were collected in a beaker. This was then transferred back to the feed, and the formed emulsion was reprocessed up to 4 times. Each experiment was repeated twice.

2.3. Droplet Size and Droplet Size Measurements. The measurement of droplet size and droplet size distribution were performed by using a Mastersizer 2000 (Malvern Instruments). Samples were diluted to 3 vol % to avoid multiple-light scattering. Each sample was prepared and tested twice at room temperature (22°C).

2.4. Interfacial Tension Measurements. The equilibrium interfacial tensions were measured using a K11-Force Tensiometer (Krüss, GmbH) equipped with a Wilhelmy plate for (i) the plain oil−water interface and (ii) at varying concentration of the surfactant. The equilibrium interfacial tension of the plain oil−water interface was equal to 24.95 ± 0.02 mN/m, whereas when the Tween20 concentration was increased from 0.01 to 2 wt % the equilibrium interfacial tension decreased from 6.04 ± 0.01 to 5.29 ± 0.02 mN/m, respectively.

2.5. Stability. To evaluate the stability of the processed emulsions, samples were stored in the laboratory at room temperature (22°C) over a period of 40 d. Since creaming occurred in most of the samples analyzed in this study, the samples were gently redispersed before remeasuring the droplet size.

2.6. CFD Simulations. Commercial Ansys 18 Fluent 18.0 was used to simulate the fluid flow into CIJM. The geometry was modeled using the Design Modeler in the Ansys Workbench and was divided in multiple connected volumes. The grid was generated using a curvature size function; the inlet tubes and the impingement zone were meshed using a Multizone method, whereas the rest of the geometry by a sweep method resulted in 2 400 000 hexahedral cells (grid element quality = 0.723 ± 0.159). Information about the velocity and energy dissipation

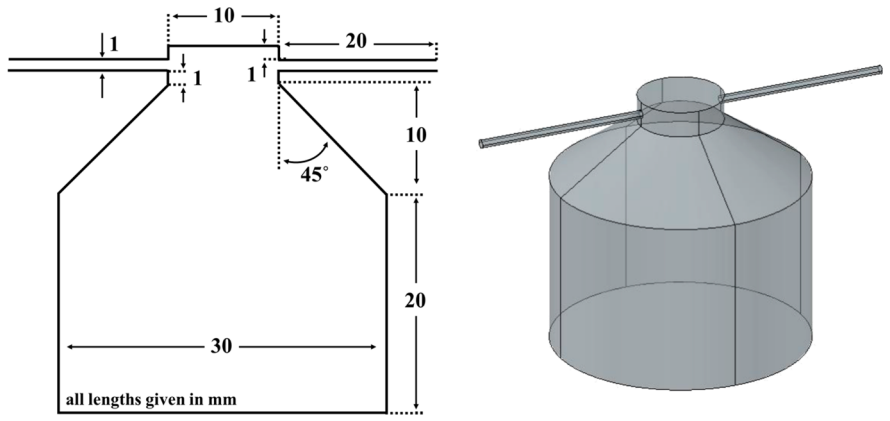

Figure 2. Schematic and three-dimensional representation of the CIJM geometry used in this study; all dimensions are given in millimeters.

DOI: 10.1021/acs.iecr.9b00634
Ind. Eng. Chem. Res. 2019, 58, 14859−14872

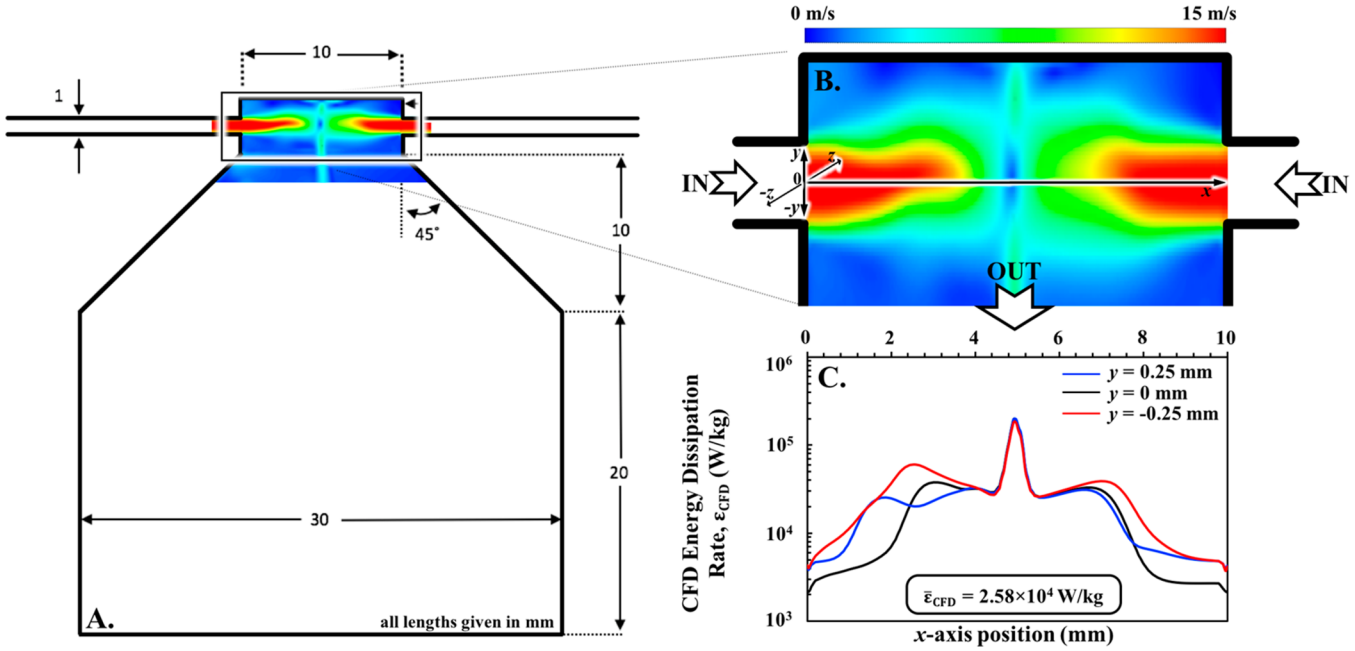

Figure 3. (A) CFD-obtained velocity contours of the simulated flow and impingement of two aqueous jets (of equal mass flow rates of 702 g/min) within the mixing chamber of the CIJM geometry used in this study. (B) Enlarged view of velocity contours within the mixing chamber of the CIJM geometry together with the *x*, *y*, and *z* axes; the *x*-axis extends from 0 to 10 mm, the *y*-axis extends from −0.5 to 0.5 mm, and the *z*-axis extends from −0.5 to 0.5 mm (*x*, *y*, *z* = 0 as shown in the schematic). (C) Energy dissipation rate (ε_{CFD}) as a function of position along the *x*-axis and at three different positions on the *y*-axis; *y* = −0.25, 0, and 0.25 mm. $\overline{\varepsilon}_{CFD}$ (2.58×10^4 W/kg) is calculated as the average of the three ε_{CFD} curves (see main text for further detail).

rate profiles at varying jet flow rate was obtained for water (density 998 kg/m^3 and viscosity 1 mPa·s). CFD simulations of the flow of two pure aqueous streams clearly model a simplified system and thus obviously do not offer insights into many of the key physical phenomena taking place during emulsification within the CIJM device, for example, droplet breakup or coalescence mechanisms. However, as the shear viscosity of (at least) the 10 wt % oil pre-emulsion is relatively close to that of pure water (Figure 1), the model does hold some value.

The Large-Eddy-Simulation (LES) model would represent a more suitable method to describe the transient phenomena taking place during mixing, but it is also acknowledged to be a highly time-intensive solving model.[15] Thus, for the purpose of this study the standard k-ε model was used to model the fluid flow. Boundary conditions of (i) constant inlet velocities for both inlet tubes, (ii) zero-gauge pressure for the outlet, and (iii) no wall slip for the walls were specified. The SIMPLE pressure–velocity coupling, the Least Squares Cell Based gradient, and second-order methods were used. Since the flow inside the geometry is unsteady, a steady-state simulation was initially run to initialize the transient calculation. Three time steps of size varying between 6 to 0.6×10^{-6} s were used. Following this procedure all the residuals fell below 1×10^{-4}.

The benefit to this study is that both the velocity contours of the simulated flow and the energy dissipation rates achieved within the CIJM geometry can be calculated by the model and then used to (at least qualitatively) first assess whether jet impingement does take place and second obtain a measure of the magnitude of the turbulence realized in relation to the inlet jet mass flow rate. Figure 3 provides an example (for W_{jet} = 702 g/min) of the approach used for the calculation of mean energy dissipation rates ($\overline{\varepsilon}_{CFD}$) along the impingement path of the jets (*x*-axis) from the CFD data. The energy dissipation rate (ε_{CFD}) along the *x*-axis, from the left entry channel to the CIJM chamber (*x* = 0 mm) to the channel on the right (*x* = 10 mm), is first calculated at three different *y*-positions (*y* = −0.25, 0, and 0.25 mm) (see Figure 3B). All three energy dissipation rate curves obtained by the simulation (see Figure 3.C) exhibit a peak (at an ε_{CFD} value of $\sim 1.8 \times 10^5$ W/kg) corresponding to a position on the *x*-axis of 5 mm, thus confirming that the jet impingement point is observed at the center of the CIJM chamber. $\overline{\varepsilon}_{CFD}$ is then calculated as the average of these three ε_{CFD} curves, corresponding, in this case (W_{jet} = 702 g/min), to be 2.58×10^4 W/kg.

3. RESULTS AND DISCUSSION

3.1. Assessment of CIJM Emulsification Capacity. In the present study, CIJM emulsification capacity is first assessed using a CFD computational approach to understand the effect of the inlet jet mass flow rate (W_{jet}) on the hydrodynamic conditions (i.e., energy dissipation rate and velocity profiles) realized within the CIJM geometry (Figure 2). The CIJM processing capacity is then further interrogated by investigating the effect of pre-emulsion droplet size and dispersed-phase content on the final emulsion microstructure.

3.1.1. Modeling of CIJM Operation. The resulting relationship between $\overline{\varepsilon}_{CFD}$ and W_{jet} (the latter corresponding to the range of jet mass flow rates investigated experimentally here) is presented in Figure 4; velocity contours for selected W_{jet} values are also shown. The velocity profiles clearly suggest that at W_{jet} < 176 g/min, the two jets do not optimally impinge, and therefore poor mixing conditions prevail. In addition to this, the CFD data show that, at low W_{jet} values (<266 g/min), the mean energy dissipation rate is relatively low and only marginally rises with increasing jet mass flow rates (Figure 4). However, for W_{jet} values above 266 g/min, $\overline{\varepsilon}_{CFD}$ increases rapidly, reaching a value of 2.58×10^4 W/kg at the highest jet mass flow rate (702 g/min).

DOI: 10.1021/acs.iecr.9b00634
Ind. Eng. Chem. Res. 2019, 58, 14859−14872

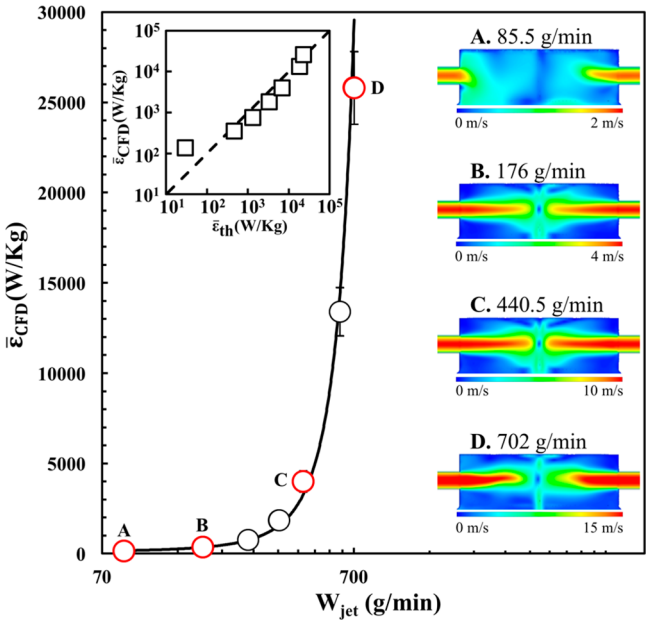

Figure 4. Mean energy dissipation rate from the CFD simulations ($\bar{\varepsilon}_{CFD}$) as a function of jet mass flow rate (W_{jet}). $\bar{\varepsilon}_{CFD}$ values are calculated as described in the main text, and error bars represent one standard deviation; where not visible, error bars are smaller than the used symbol. Velocity profiles derived from the CFD simulations are also provided as insets for selected W_{jet} values; (A) 85.5, (B) 176, (C) 440.5, and (D) 702 g/min. (inset) Graph shows $\bar{\varepsilon}_{CFD}$ against theoretical mean energy dissipation rates ($\bar{\varepsilon}_{th}$; eq 4), across the range of W_{jet} values used in the present study.

The inset plot in Figure 4 compares the calculated $\bar{\varepsilon}_{CFD}$ values to the theoretical mean energy dissipation rates ($\bar{\varepsilon}_{th}$) as predicted by eq 4 for a pure aqueous phase. The two mean energy dissipation rates show excellent agreement, with the only exception being the $\bar{\varepsilon}_{CFD}$ values at the lowest jet mass flow rate. Despite this, it is clear that, within the range of W_{jet} values where efficient mixing within the CIJM cavity is to be expected, the CFD simulation can sufficiently estimate the CIJM flow dynamics as predicted by theory.

The reason for the compromised CIJM operation at low W_{jet} values is suggested to relate to the geometry of the device used here. Compared to CIJM configurations used elsewhere in either experimental or computational studies on CIJM,[15−17,19] the geometry employed here presents a different geometrical design. For the purpose of this investigation, the CIJM cavity was devised with a longer jet-to-jet distance and a larger outlet diameter in an attempt to overcome the backpressure developed during the emulsification of more concentrated emulsions (Sections 3.2 and 3.3). These differences in the geometry of the devices are potentially responsible for the failure of the jets to collide at the lowest W_{jet} values. Differently, the reduced jet-to-jet distance and narrower outlet of the configurations used elsewhere[15−17,19] resulted in jet collisions taking place over the entire range of tested jet mass flow rates. Although one must note that, at higher W_{jet} (≥176 g/min), the mixing capacity of the CIJM configuration employed here appears to align with that of the previously used geometry; a peak in the ε_{CFD} profiles at the point of jet impingement as well as a similar exponential rise in $\bar{\varepsilon}_{CFD}$ with increasing W_{jet} have both been reported in these past studies.[15−17,19]

3.1.2. The Effect of the Pre-Emulsion Droplet Size on the CIJM Emulsification Capacity. The effect of varying the initial

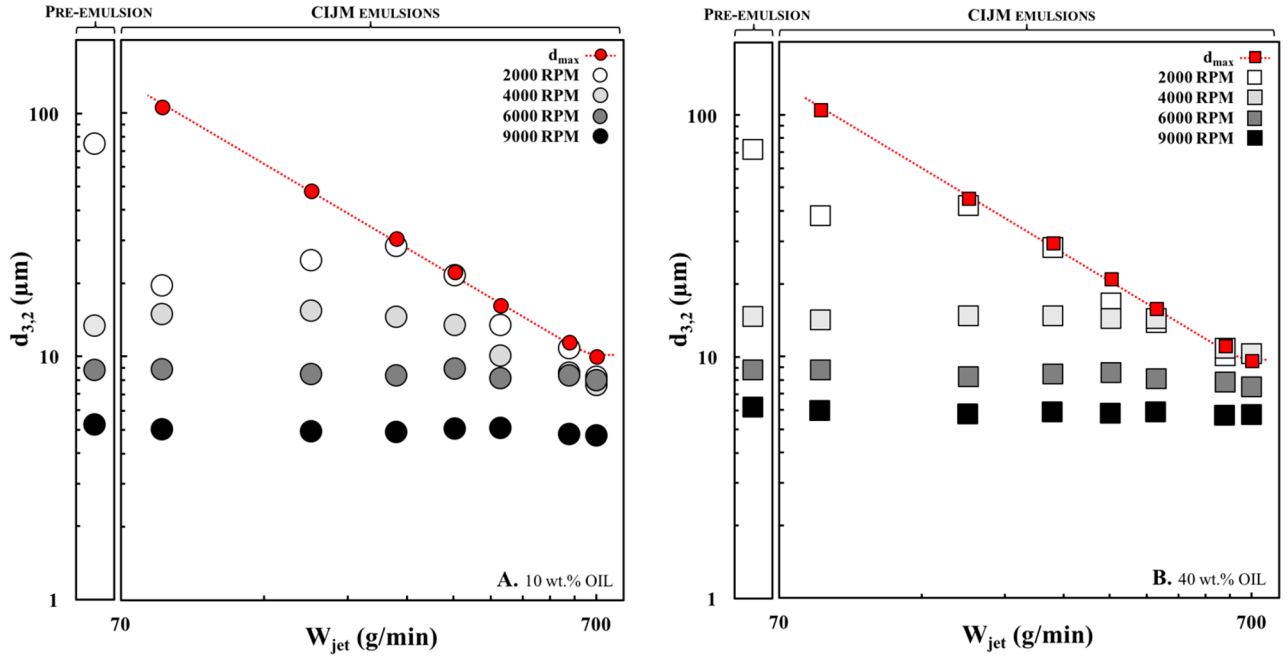

Figure 5. Final emulsion Sauter mean diameter ($d_{3,2}$) as a function of jet mass flow rate (W_{jet}), following CIJM processing of pre-emulsions (original droplet sizes for these are also given) in the presence of 1 wt % Tween20. (A) CIJM treatment of 10 wt % oil mass fraction pre-emulsions prepared using a high shear mixer at 2000 (○), 4000 (light gray ●), 6000 (dark gray ●), and 9000 (●) RPM. (B) CIJM treatment of 40 wt % oil mass fraction pre-emulsions prepared using a high shear mixer at 2000 (□), 4000 (light gray ■), 6000 (dark gray ■), and 9000 (■) RPM. Red full circles (●) and red full squares (■) represent the maximum stable droplet diameter d_{max} (μm) calculated at each corresponding W_{jet} using eq 4 for pre-emulsions of 10 and 40 wt % oil mass fractions, respectively; in both cases dotted curves are only shown as a guide. All data points are mean values ($n = 2$), and error bars represent one standard deviation of the mean; where not visible, error bars are smaller than the used symbol.

DOI: 10.1021/acs.iecr.9b00634
Ind. Eng. Chem. Res. 2019, 58, 14859−14872

droplet size of the o/w pre-emulsions (possessing either 10 or 40 wt % oil mass fractions, respectively) processed through the CIJM configuration on the emulsification capacity of the device (in terms of the average droplet size ($d_{3,2}$) of the corresponding final emulsion produced) is shown in Figure 5. The premixing conditions in the used high-shear mixer were chosen to obtain pre-emulsions with significantly different initial average droplet sizes, which were then passed through the CIJM device using a range of W_{jet} values (85.5−702 g/min). The data presented in Figure 5 clearly show that pre-emulsions prepared at 2000 rpm underwent the greatest change in droplet diameter upon CIJM processing. For both the 10 and 40 wt % oil content pre-emulsions prepared at 2000 rpm ($d_{3,2} \approx 73$ μm), the original droplet size is initially reduced (at the lowest mass flow rate). As W_{jet} values increase, this droplet size reduction becomes less pronounced only to again sharply increase at higher CIJM mass flow rates. Pre-emulsions prepared at 4000 rpm ($d_{3,2} \approx 14$ μm) deviated from this behavior, and changes to the original droplet size were only observed at the highest mass flow rates for both oil contents. In contrast to the last two systems, pre-emulsions prepared at 6000 ($d_{3,2} \approx 9$ μm) and 9000 rpm ($d_{3,2} \approx 6$ μm) did not undergo any size change throughout the range of W_{jet} values and regardless of the oil mass fraction in the system.

Droplet size distribution (DSD) data confirmed these observations, Figure S.1A,B. On the one hand, the DSD of both the 10 wt % pre-emulsions prepared at 2000 and 4000 rpm decreased appreciably when processed at the highest W_{jet} (702 g/min), Figure S.1A. On the other hand, insignificant changes in terms of DSD were observed when pre-emulsions prepared at both 6000 and 9000 rpm were processed through the CIJM, Figure S.1B. Analogous trends were also observed for the DSD of 40 wt % (pre-) emulsions (not shown).

The erratic behavior observed while processing the pre-emulsions with the largest droplet size (2000 rpm) through the CIJM geometry is hypothesized to relate to the poor mixing conditions and deficient jet impingement that take place at lower W_{jet} and as revealed by the CFD model (Section 3.1.1). However, the processing capacity of the CIJM device is not only determined by W_{jet}. The data in Figure 5 suggest that the CIJM emulsification potential is also very much dependent on the original droplet size of the to-be-processed pre-emulsion. It appears that a clear threshold value in terms of the pre-emulsion original size ($d_{3,2}$) exists in order for CIJM intervention to be successful; in this case, it is a $d_{3,2}$ value of ∼10 μm. Above this threshold it is possible for CIJM processing to impact and therefore reduce the original pre-emulsion droplet size, providing of course that the used W_{jet} is high enough. Conversely, processing pre-emulsions with droplet sizes lower than this threshold does not lead to any change in the original droplet size regardless of the hydrodynamic conditions (i.e., W_{jet}).

The dependency of both the pre-emulsion droplet size and jet mass flow rate on the CIJM emulsification capacity can also be explained using the concept of maximum stable droplet diameter (d_{max}). Extensively utilized in literature to describe the balance between deforming and restoring forces acting on droplets subjected to turbulent flow, d_{max} is essentially the (mean) maximum droplet diameter that is able to retain a stable size under the imposed hydrodynamic conditions.[22] A previous study[23] reports that, during the processing of relatively low viscosity systems, CIJM is expected to operate under TI flow regime conditions; this is indeed confirmed in the latter parts of the present work for both the 10 and 40 wt % oil content systems studied here. d_{max} can be therefore estimated for each jet mass flow rate W_{jet} using eq 2; the calculated d_{max} values are also provided in Figure 5.

For both oil content pre-emulsions prepared at 2000 rpm, final emulsion mean droplet sizes ($d_{3,2}$) produced at low jet mass flow rates (W_{jet} < 266 g/min for the 10 wt % and W_{jet} < 176 g/min for the 40 wt % oil content systems, respectively) initially assume values smaller than the corresponding d_{max}. However, as W_{jet} is increased further and CIJM is expected to operate under optimal emulsifying conditions, final emulsion $d_{3,2}$ begins to decrease and closely follows the theoretically calculated d_{max}. The onset of the alignment between $d_{3,2}$ and d_{max} for pre-emulsions prepared at 4000 rpm is suppressed and only occurs at high jet mass flow rates ($W_{jet} \geq 352.75$ g/min), regardless of oil content in the system.

Finally, pre-emulsions prepared at 6000 and 9000 rpm pass through the CIJM geometry to give final emulsions of practically unchanged droplet sizes. Thus, these systems, as previously discussed due to their much smaller pre-emulsion droplet sizes, are seemingly unaffected by the induced turbulent conditions and understandably do not exhibit any alignment with any of the corresponding d_{max} values; one could argue that a negligible size reduction can be observed for pre-emulsions produced at 6000 rpm when subjected to the highest jet mass flow rate (702 g/min), but it is probably more realistic to treat this decrease as both experimentally and statistically insignificant.

Overall, the relation between final emulsion $d_{3,2}$ and theoretical d_{max} appears to support the impact on the CIJM emulsification capacity of both the original pre-emulsion droplet size and jet mass flow rate that was proposed earlier. It is suggested that the close agreement between final emulsion $d_{3,2}$ and theoretical d_{max} is in itself a good indicator of successful CIJM emulsification capacity. In keeping with the preceding discussion on the CIJM emulsification potential, $d_{3,2}/d_{max}$ alignment is only realized for pre-emulsions with droplet sizes similar to or greater than the theoretical d_{max} value corresponding to the hydrodynamic conditions produced by the used W_{jet}; providing also that the employed jet mass flow rate is high enough to encourage successful jet impingement that is also associated with an increased energy dissipation rate. The interplay between $d_{3,2}$ and d_{max} is probably better demonstrated in Figure 6, where these two droplet dimensions are plotted against one another for systems of varying oil content and pre-emulsion droplet sizes processed through the CIJM device over a range of W_{jet}. The data suggest that, when the characteristics of the pre-emulsions (i.e., in terms of oil content and droplet size) and the processing conditions that these are subjected to (i.e., in terms of W_{jet}) are both controlled to allow for the successful emulsification performance of the CIJM geometry, then final emulsion $d_{3,2}$ and d_{max} exhibit a liner dependency ($d_{3,2} = c\, d_{max}$). Since the pioneering study by Sprow,[24] the linear relationship between the Sauter and the maximum stable droplet diameters has been extensively reported for a number of conventional emulsification techniques (e.g., high-shear and static mixers, simple agitated tanks, etc.), and the value of parameter c has been found to vary between 0.38 and 0.70.[25,26] In the present study, the slope of the linear dependency between $d_{3,2}$ and d_{max} is found to be 0.86 (±0.10); this is shown in Figure 6 as a solid straight line, with the shaded area denoting the minimum ($c - \sigma$) and maximum ($c + \sigma$) slopes, where σ is the standard deviation. It is not clear at this stage why the c value for the CIJM device is higher than in other emulsification techniques or even whether this difference indicates to variations in some tangible processing

DOI: 10.1021/acs.iecr.9b00634
Ind. Eng. Chem. Res. 2019, 58, 14859−14872

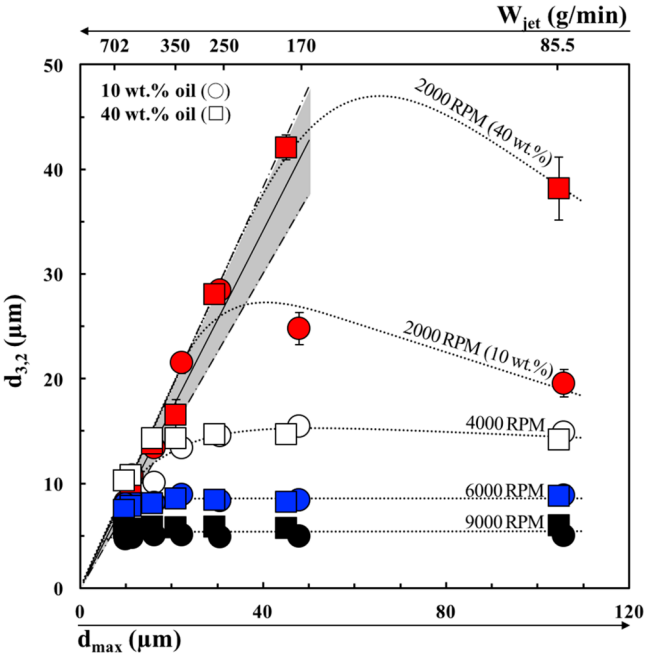

Figure 6. Final emulsion Sauter mean diameter ($d_{3,2}$) following CIJM processing of pre-emulsions (initially prepared using the high-shear mixer at RPM values as indicated on the graph) with 10 wt % (circles) and 40 wt % (squares) oil mass fractions, respectively, and in the presence of 1 wt % Tween20, as a function of the maximum stable diameter (d_{max}) and jet flow rate (W_{jet}). Dotted curves are only shown as a guide. Solid straight line (and shaded area) denotes a liner dependency between $d_{3,2}$ and d_{max} (see main text for further detail). All data points are mean values (n = 2), and error bars represent one standard deviation of the mean; where not visible, error bars are smaller than the used symbol.

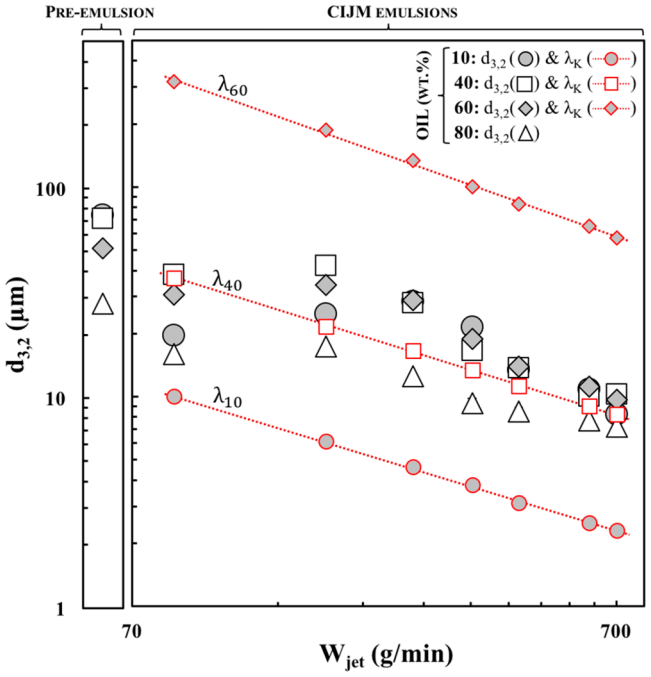

Figure 7. Final emulsion Sauter mean diameter ($d_{3,2}$) as a function of jet mass flow rate (W_{jet}), following CIJM processing of pre-emulsions (original droplet sizes for these are also given) with 10 (●), 40 (□), 60 (◆), and 80 (△) wt % oil content and in the presence of 1 wt % Tween20. Red outline symbols represent the theoretical Kolmogorov eddy sizes (λ_k; eq 1) corresponding to the characteristics of the 10, 40, and 60 wt % dispersed-phase mass fraction systems. Dotted lines are only shown as a guide. All data points are mean values (n = 2), and error bars represent one standard deviation of the mean; where not visible, error bars are smaller than the used symbols.

characteristics associated with the operation of the device (compared to that in conventional methods). Nonetheless, it must also be noted that establishing a clear correlation between $d_{3,2}$ and d_{max} may not always be possible, as the dependency may vary randomly and more importantly not always be linear.[26]

3.2. CIJM Emulsification Performance. On the basis of the findings of the previous section, to evaluate the CIJM emulsification performance for a range of processing and formulation parameters (e.g., hydrodynamic conditions, dispersed-phase mass fractions, and concentration of the emulsifier), all pre-emulsions to be processed through the CIJM geometry were produced using as mild high-shear mixing conditions as possible. This to ensure CIJM performance is not jeopardized by the pre-emulsion droplet size. The 10 and 40 wt % oil pre-emulsions were prepared (as previously) in the high-shear mixer at 2000 rpm (for 3 min), whereas for the more concentrated systems, both 60 and 80 wt %, slightly more intense mixing was required (3500 rpm for 3 min) to obtain a well-dispersed system; processing the latter more concentrated systems at 2000 rpm resulted in rapid phase separation, which took place prior to commencing CIJM processing. As a result, the 10 and 40 wt % pre-emulsions had a similar average droplet size (75 and 72 μm, respectively), while the 60 and 80 wt % systems possessed initial droplet sizes of 52 and 28 μm, respectively, Figure 7; in all cases pre-emulsion droplet size was maintained above the threshold of ~10 μm (see previous section).

3.2.1. Effect of Oil Mass Fraction. The Sauter diameters $d_{3,2}$ of the final emulsions produced by processing pre-emulsions containing a wide range of dispersed-phase mass fractions (10–80 wt %) through the CIJM device at varying jet mass flow rates W_{jet} are presented in Figure 7. Overall, the behavior of systems with varying dispersed-phase mass fractions upon CIJM processing was very similar. At low W_{jet}, final emulsion droplet size was initially decreased, with this reduction becoming less evident at slightly higher mass flow rates (176 g/min) but eventually increasing to give a more abrupt reduction in $d_{3,2}$ once W_{jet} became high enough (W_{jet} > 266 g/min). The latter range of jet mass flow rates was previously identified to correspond to optimal CIJM operation, and under the hydrodynamic conditions imposed in this case the progressive increase in the dispersed-phase mass fraction from 10 to 60 wt % content did not result in significant variations in the Sauter diameters of the final emulsions. The 80 wt % oil content emulsion exhibited lower final droplet sizes than the other systems, with these differences becoming less pronounced at higher W_{jet} (≥615 g/min), where all systems exhibited similar droplet sizes (~7–9 μm) regardless of dispersed-phase fraction.

The pre-emulsion DSDs maintained their monodisperse characteristics when processed through the CIJM for all the dispersed-phase mass fractions, Figure S.2A,B. Regardless on both the monodispersity of the pre-emulsions and the oil content, all systems showed a similar DSD when processed under the highest CIJM hydrodynamic conditions.

At constant energy input and emulsifier content, emulsion droplet size should be expected to increase with higher dispersed-phase mass fractions due to (among others): a potential increase in the frequency of droplet collisions and

DOI: 10.1021/acs.iecr.9b00634
Ind. Eng. Chem. Res. 2019, 58, 14859–14872

thus higher rates of coalescence; the increased viscosity, which hinders droplet breakup; the increase in total interfacial area and the subsequently increased likelihood of a reduction in emulsifier interfacial adsorption rates.[27,28] This dependency has been indeed observed in conventional emulsification processes; for example, high-pressure homogenization was reported[29] to produce emulsions (at a constant surfactant concentration) with consistently larger droplet sizes as the dispersed-phase mass fraction was increased from 10 to 50 wt % and throughout the range of homogenization pressures used. However, previous studies on CIJM reported[19] that, under fully turbulent conditions, the hydrodynamic environment established within the CIJM geometry was able to produce emulsions of similar droplet sizes independently from either the type of surfactant or dispersed-phase volume fraction used, albeit the latter was not greatly varied (5 and 10 v/v %).

Although this aligns with the minimal effect of oil content observed here for systems of up to 60 wt % oil, it does not support the behavior exhibited by the 80 wt % dispersed-phase emulsions. One could argue that the lower final emulsion $d_{3,2}$ value of the 80 wt % oil content system is because the pre-emulsion droplet size for these systems was lower as well. It is proposed that this is not the case and that the observed droplet size reduction is instead due to a change in the turbulent flow regime, which has been previously reported to take place as a result of increasing the dispersed-phase mass fraction.[6] In highly concentrated systems (ϕ > 75%), droplet disruption does not take place due to turbulence, which is mostly suppressed because of the large number of droplets; this has also been observed for lower-fraction systems (up to 15 wt %), which however possess much smaller droplet sizes (~200 nm), to again give a large overall number of droplets.[30] Alternatively droplet breakup in this case tends to be driven by hydrodynamic interactions between neighboring droplets.[5]

To determine whether a transition from a TI regime to a TV regime takes place for the systems studied here, the $d_{3,2}$ values of all emulsions up to an oil content of 60 wt % were compared with theoretically calculated Kolmogorov eddy size λ_k (estimated by eq 1; Figure 7); the λ_k value corresponding to the 80 wt % oil systems cannot be calculated by eq 1, since at such high dispersed-phase contents, turbulence is mostly suppressed by the presence of a high population of droplets.[5,31] The data presented in Figure 7 confirm that such a flow transition occurs, in fact proposing that it takes place as the oil content of the emulsions is increased from 40 to 60 wt %. In a previous study utilizing two conventional rotor-stator emulsification methods, a transition from TI to TV regime was also detected at dispersed-phase mass fractions between 40 and 60 wt %.[5] However, literature also suggests that emulsion droplets generated under TV conditions would be typically expected to have smaller droplet sizes compared to those produced in a TI regime,[32] a hypothesis that is not supported here. A possible explanation for this lays in the dual contribution that an increase in emulsion viscosity (or in our case an increase in dispersed-phase mass fraction) has on both d_{max} and λ_k. On the one hand, as emulsion viscosity is raised, d_{max} (as established during emulsification within a TV-regime; eq 3) is reduced, thus favoring droplet fragmentation. On the other hand, the same viscosity increase will also suppress the formation of small eddies (eq 1), and as a consequence the minimum (lower limit) droplet size that can be formed is elevated. Either of these two scenarios will prevail when flow conditions (TI or TV regime) are fully established. However, for the systems studied here, these two opposite effects appear to offset one another, thus leading to similar droplet sizes between the systems of low to moderate (10 and 40 wt %; TI regime) and high (60 wt %; TV regime) dispersed-phase contents. This potentially also denotes that, although a transition from a TI to TV regime does take place within the dispersed-phase mass fraction range from 40 to 60 wt %, the latter (TV) turbulent flow is probably not yet fully established at the 60 wt % oil content.

The interplay between emulsion dispersed-phase content and the CIJM hydrodynamic conditions was explored further by recirculating all systems (formed after one pass) through the device for a total of four passes. As such, the time that each system experiences the hydrodynamic conditions imposed within the CIJM geometry is extended without changes to the jet mass flow rate, which in this case was fixed at 352.75 g/min; this W_{jet} value is within the previously determined optimum CIJM emulsification performance range but, at the same time, not too high to overshadow any effects arising as a result of dispersed-phase content. The Sauter diameters of the final emulsions produced following multiple passes through the CIJM geometry are presented in Figure 8.

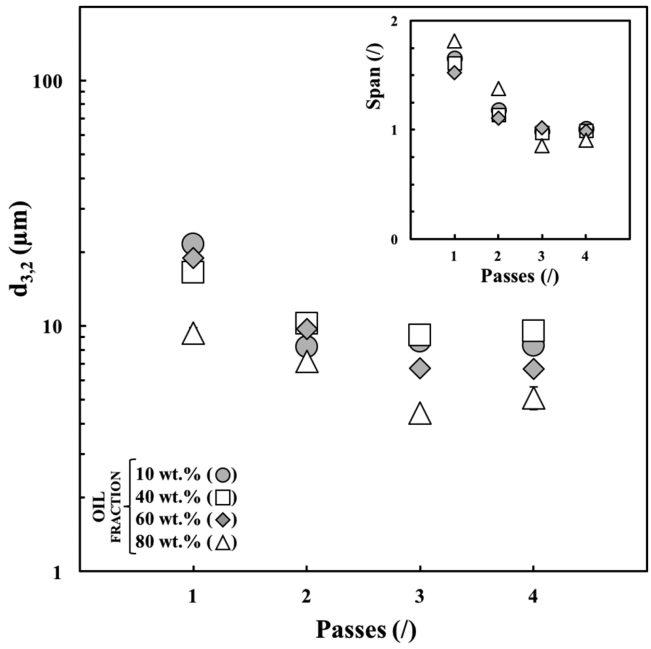

Figure 8. Sauter diameter ($d_{3,2}$) and span values (inset graph) of emulsions (in the presence of 1 wt % Tween20) with varying oil content as a function of the number of passes through the CIJM geometry at a fixed jet flow rate of 352.75 g/min. All data points are mean values (n = 2), and error bars represent one standard deviation of the mean; where not visible, error bars are smaller than the used symbols.

The obtained data show that both the 10 and 40 wt % dispersed-phase emulsions reach a minimum droplet size after the second pass through the geometry and that, despite their different oil content, they both maintain similar $d_{3,2}$ values. However, the average droplet sizes for the 60 and 80 wt % oil content emulsions still decrease up to the third pass; both systems also display smaller $d_{3,2}$ values in comparison to the less-concentrated systems (10 and 40 wt % dispersed phase). These results confirm that emulsions formed under a TV regime (60 wt % oil content) or in the presence of a significantly high population of droplets (80 wt % oil content) will possess smaller

DOI: 10.1021/acs.iecr.9b00634
Ind. Eng. Chem. Res. 2019, 58, 14859−14872

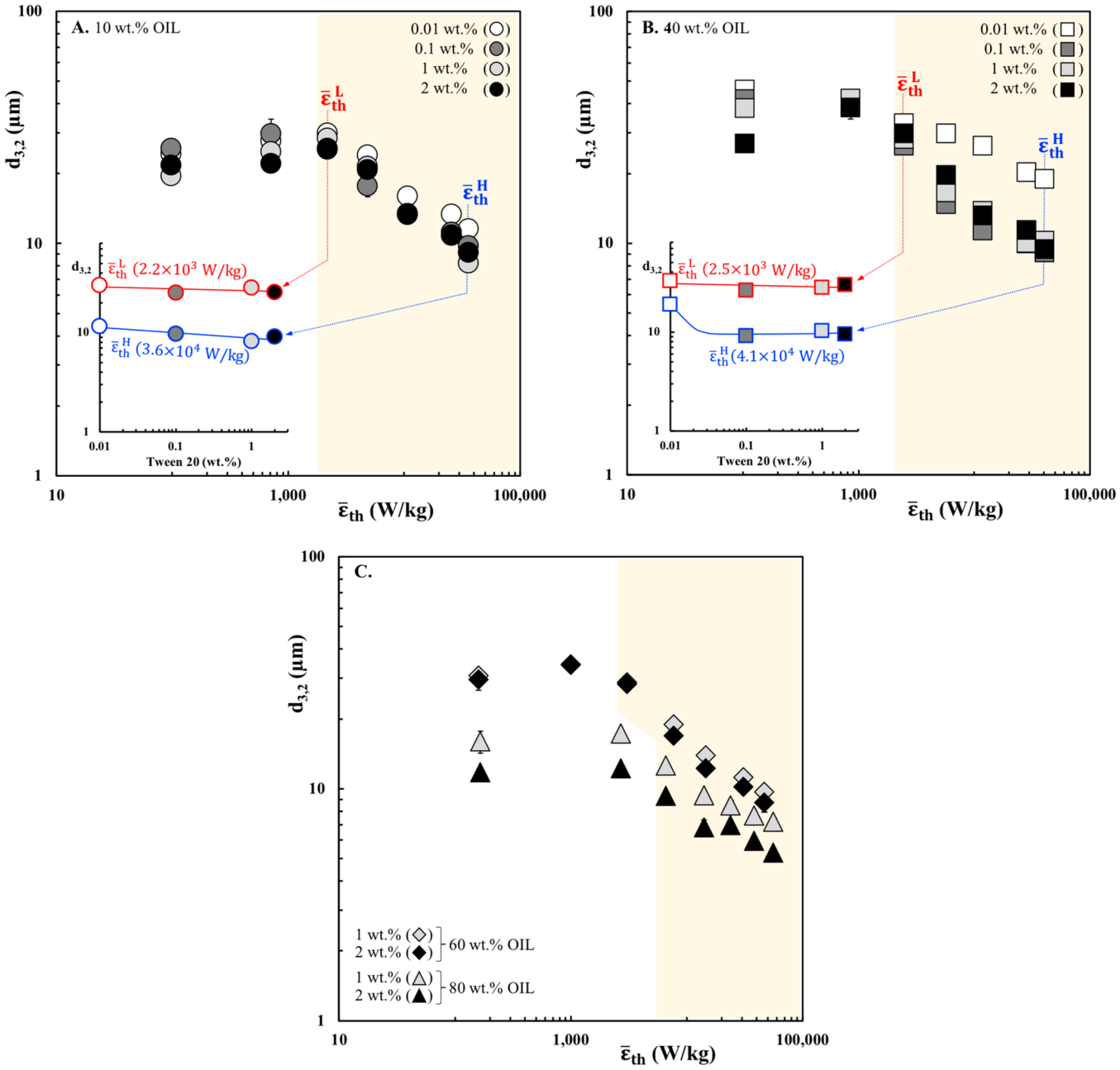

Figure 9. Final emulsion Sauter mean diameter ($d_{3,2}$) as a function of the theoretical mean energy dissipation rate ($\bar{\varepsilon}_{th}$; eq 4) following a single pass during CIJM processing of pre-emulsions with of 10 wt % (A), 40 wt % (B), and 60 or 80 wt % (C) oil mass fractions in the presence of Tween20 concentrations ranging from 0.01 to 2 wt %. (inset graphs) The dependency of final $d_{3,2}$ on Tween20 concentration at fixed low ($\bar{\varepsilon}^{L}_{th}$) and high ($\bar{\varepsilon}^{H}_{th}$) mean energy dissipation rates (see main text for further detail). All data points are mean values ($n = 2$), and error bars represent one standard deviation of the mean; where not visible, error bars are smaller than the used symbols.

droplets than those generated under TI conditions (10 and 40 wt % oil content), even though the processing conditions used in either case are indeed similar.[6] Therefore, it is also suggested that, although the transition from a TI to a TV-regime (between 40 and 60 wt % dispersed phase) is perhaps not fully realized after a single pass through the CIJM geometry (see earlier discussion), increasing the residence time of the 60 wt % oil content within the high-energy dissipation zone of the device assists in fully establishing the Turbulent-Viscous flow regime conditions.

CIJM recirculation was also found to impact on the droplet size distribution of the emulsions, Figure S.3A,B, perhaps to a more significant extent than the effect that multipassing had on emulsion average droplet size. Regardless of dispersed-phase mass fraction and number of passes, the droplet size distributions for all systems remained monomodal; the span values for these as a function of the number of passes through the CIJM geometry are presented in Figure 8. Independent from the oil mass fraction, all size distributions became narrower, exhibiting a reduction in the initial span of 1.4−1.6 (first pass) to values in the range of 0.8−1 (after the third pass); negligible or no changes were observed after the fourth pass. The effect of extending the residence time within the CIJM processing environment has been previously studied for emulsions of much lower dispersed-phase contents (up to a volume fraction of 0.1).[19] Similarly to the findings reported here, the past study

DOI: 10.1021/acs.iecr.9b00634
Ind. Eng. Chem. Res. 2019, 58, 14859−14872

concluded that the major emulsion microstructure change occurring during multipassing is the narrowing of the droplet size distribution and that the average droplet size is only mildly influenced by the number of passes. This behavior has also been reported by studies evaluating the emulsification performance during high-pressure homogenization and microfluidisation, where in both cases the droplet size distribution (rather than droplet size) was primarily affected by recirculation.[33,34]

3.2.2. Effect of Surfactant Concentration. The effect of surfactant (Tween20) concentration on the Sauter diameter $d_{3,2}$ of emulsions possessing a range of oil mass fractions (10−80 wt %) and produced within the CIJM device under varying hydrodynamic conditions (in this case represented by the theoretical mean energy dissipation rate $\overline{\varepsilon}_{th}$) is shown in Figure 9. Surfactant concentrations of 0.01, 0.1, 1, and 2 wt % were used for the preparation of all systems; however, emulsions with a higher dispersed-phase content (60 and 80 wt %) at the lower Tween20 concentrations (0.01 and 0.1 wt %) phase separated almost immediately following premixing (pre-emulsion formation), and CIJM processing in this case was not possible. All other pre-emulsions were stable enough to pass through the CIJM geometry, and final emulsion $d_{3,2}$ values, regardless of oil content or surfactant concentration, exhibited overall the same dependency (see Figure 9) on hydrodynamic conditions as discussed earlier (e.g., Figure 7); that is, emulsification performance is shown to be jeopardized at low jet mass flow rates (or similarly here at low $\overline{\varepsilon}_{th}$), and the onset of optimum CIJM operation is only achieved once this is appropriately increased. The range where successful CIJM emulsification performance is expected to be realized corresponds to the shaded area(s) also shown in Figure 9. The discussion in this section will only focus on emulsions produced within this optimal CIJM processing window.

Emulsion $d_{3,2}$ dependency on Tween20 concentration within the CIJM optimal processing region is first evaluated at two fixed but dissimilar $\overline{\varepsilon}_{th}$ values representing the low-energy dissipation rate at the onset of the CIJM optimal operating conditions ($\overline{\varepsilon}_{th}^{L}$) and the highest-energy dissipation rate ($\overline{\varepsilon}_{th}^{H}$) employed. Because of the stability issues exhibited by the 60 and 80 wt % oil content systems at the lower Tween20 concentrations, the aforementioned analysis is only meaningful for the 10 and 40 wt % dispersed-phase emulsions; the behavior of the latter systems is shown in the inset graphs of Figure 9A,B, respectively.

The droplet size of the 10 wt % o/w emulsions is reduced from ∼30 μm to a minimum value of ∼10 μm, independently from the amount of surfactant in the system (Figure 9A). As also shown by the data in the inset graph, varying the surfactant concentration in systems produced under fixed, either mild ($\overline{\varepsilon}_{th}^{L}$) or fully ($\overline{\varepsilon}_{th}^{H}$) turbulent, hydrodynamic conditions does not result in emulsions with considerably different droplet sizes. For the 40 wt % systems, differences in emulsion droplet size for varying surfactant contents were more evident (Figure 9B). The lowest Tween20 concentration (0.01 wt %) was clearly shown to result in the highest droplet sizes, while all other formulations (0.1 to 2 wt %) all culminated in similar $d_{3,2}$ values independently from $\overline{\varepsilon}_{th}$. The extent of the difference in the droplet sizes between these two subgroups became progressively more marked as the energy dissipation rate was increased (Figure 9B). While at $\overline{\varepsilon}_{th}^{L}$ emulsion droplet sizes remain practically unaffected by variations in the amount of Tween20, at $\overline{\varepsilon}_{th}^{H}$ the Sauter diameter of the systems decreases from ∼20 μm (at a Tween20 concentration of 0.01 wt %) to a plateau value of ∼10 μm (for a surfactant content greater or equal to 0.1 wt % of Tween20). Finally, the dependency of $d_{3,2}$ on $\overline{\varepsilon}_{th}$ for both the 60 and 80 wt % systems containing either a 1 or 2 wt % surfactant concentration is shown in Figure 9C. Whereas this Tween20 concentration variation results in negligible changes to the droplet sizes of the 60 wt % o/w emulsions, the same surfactant increase in the 80 wt % oil content systems produced droplets of consistently smaller $d_{3,2}$ values over the entire range of $\overline{\varepsilon}_{th}$.

Overall, it appears that the capacity of the CIJM device to reduce the size of emulsion droplets is heavily affected by surfactant availability, which, within the context of the present discussion, is essentially the surfactant concentration relative to the dispersed-phase content. CIJM processing of formulations, where surfactant availability is low, will produce emulsions with a final droplet size that, although affected by the mixing conditions imposed, is primarily driven by surfactant concentration and dispersed-phase content, that is, formulation rather than processing characteristics. Conversely, CIJM treatment of formulations of high surfactant availability will produce emulsions with droplet sizes that are predominantly governed by the hydrodynamic conditions established during processing and only marginally depend on formulation attributes.

The existence of these surfactant-poor and surfactant-rich regimes has been previously reported for conventional emulsification turbulent processing (high shear mixing, homogenization, microfluidisation), both when either the two oil and aqueous immiscible phases or a pre-emulsion are treated and for a range of species offering interfacial stabilization (surfactants, proteins, and particles).[35−38] In all cases two well-defined regimes have been observed in terms of the dependence of $d_{3,2}$ on surfactant/emulsifier concentration; at low concentrations, emulsion droplet size is highly sensitive to the amount of surfactant/emulsifier present in the system, and it relates to the extent of droplet coalescence events, while at high concentrations $d_{3,2}$ is practically independent of surfactant/emulsifier content and is mostly determined by the degree of drop breakup as imposed by processing conditions.[35,36,38] Increasing the dispersed (oil) phase fraction in the system is suggested to affect droplet size behavior in both the surfactant-poor and surfactant-rich regimes in two ways. Increasing oil content will accelerate coalescence events, because of the subsequent increase in the frequency of droplet collisions, and thus droplet size is expected to also increase.[30,37] However, at higher dispersed-phase fractions, the effective viscosity of the emulsion is also increased, and consequently, as turbulent intensity is reduced, coalescence efficiency and therefore the rate of coalescence events would tend to decrease.[30]

In an attempt to further explore the dependency of dispersed-phase content on emulsion droplet size, the $d_{3,2}$ values achieved within the optimal CIJM processing window (shaded region in the main plots of Figure 9) are presented in Figure 10 in terms of fractional droplet size reduction ($d_{3,2}/d_o$). The $d_{3,2}/d_o$ quantity is the ratio of the droplet size achieved for a given system produced under a specific $\overline{\varepsilon}_{th}$ value ($d_{3,2}$) over the droplet size of the same system but as realized following processing at the low-energy dissipation rate ($\overline{\varepsilon}_{th}^{L}$) at the onset of the CIJM optimal operating conditions (d_o). $d_{3,2}/d_o$ is a useful measure of the CIJM emulsification performance as, rather than assessing emulsion formation in terms of achieved droplet size, it evaluates the droplet reduction capacity of the device with reference to the droplet size initially obtained upon processing under the mildest operating conditions that still fall within the predetermined optimal operation of the CIJM geometry. Droplet size data for all emulsions are in this way effectively "normalized" and thus

DOI: 10.1021/acs.iecr.9b00634
Ind. Eng. Chem. Res. 2019, 58, 14859−14872

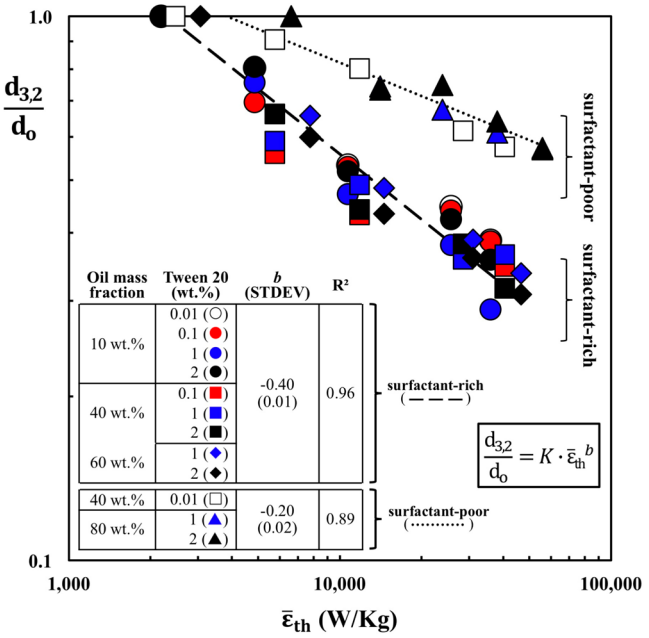

Figure 10. Fractional droplet size reduction ($d_{3,2}/d_o$) as a function of the mean energy dissipation rate ($\bar{\varepsilon}_{th}$) realized during CIJM processing of pre-emulsions with varying dispersed phase and surfactant (Tween20) content (detail on both these is given on the graph). Lines shown are the best fit of the two data clusters to a simple power law model (see main text for further detail). (inset) Table provides detail about the quality of the fit to the power law model.

can be cross-compared regardless of their dispersed phase or surfactant content. Assessing the interplay between $d_{3,2}/d_o$ and $\bar{\varepsilon}_{th}$ confirms the occurrence of the surfactant-poor and surfactant-rich regimes discussed earlier (Figure 10). The data form two clusters of behavior that correspond to either a surfactant-poor or surfactant-rich regime, with both groups exhibiting a power law dependency with $\bar{\varepsilon}_{th}$; data within the two clusters were fitted to a simple power law model ($\frac{d_{3,2}}{d_o} = K \cdot \bar{\varepsilon}_{th}^{\,b}$), with values for the exponents b and for R^2 also given (Figure 10). Analysis of the data in Figure 10 further reveals that, in terms of emulsion droplet size reduction capacity, CIJM processing is practically independent from the dispersed-phase content in the systems. This suggests that, although these systems do possess droplet sizes that are determined by both processing attributes and formulation-specific characteristics, the rate of droplet size reduction achieved within the CIJM device as a function of the generated energy dissipation rate $\bar{\varepsilon}_{th}$ is unaffected by either of the dispersed phase or surfactant content alone but, instead, is primarily driven by surfactant availability, as jointly determined by both these quantities.

3.2.3. Long-Term Emulsion Stability. The long-term stability of emulsions with a range of surfactant concentrations (0.01−2 wt %) and dispersed-phase mass fractions (10−80 wt %) produced using the CIJM device was evaluated over a period of 40 d. All systems were produced at a fixed jet mass flow rate of 352.75 g/min, which is within the previously determined optimum CIJM emulsification performance range, and they were stored at room temperature (22°C) over a period of 40 d. The Sauter mean diameters for systems of increasing dispersed-phase content both immediately after CIJM processing and following the 40 d storage period are presented in Figure 11 as a function of surfactant concentration. Selected droplet size distribution curves at both time intervals for emulsions stabilized by 2 wt % of Tween20 and for each of the oil mass fractions studied here are also provided as insets to the main graphs.

The $d_{3,2}$ data for the 10 wt % oil content emulsions (Figure 11A) clearly demonstrate that the droplet size of these systems remained (within experimental error) unchanged during storage regardless of the surfactant concentration used. The inset graph in Figure 11A further confirms the high stability of these systems over the 40 d storage period. As the dispersed-phase content is increased to 40 wt % (Figure 11B), emulsion stability becomes dependent on surfactant content. Emulsions with the lowest surfactant content (0.01 wt % Tween20) phase separated during storage, while systems with 0.1 wt % Tween20 exhibited an increase in droplet size (from 14.7 to 29.1 μm) during storage. Therefore, although the latter systems retained an emulsion microstructure, the occurrence of coalescence during storage was not avoided, and their stability was jeopardized. However, formulations with higher surfactant concentrations (1−2 wt %) were stable throughout the storage period (Figure 11B). Finally, emulsions of either 60 or 80 wt % oil mass fractions exhibited the same stability behavior during storage (Figure 11C,D). Although as previously mentioned, CIJM processing of emulsions at these dispersed-phase fractions was not achievable at the lower surfactant concentrations (0.01 and 0.1 wt % Tween20), increasing the surfactant content (≥1 wt %) resulted in practically unchanged mean droplet sizes and droplet size distribution curves during storage.

It is worth noting that the behavior discussed earlier in terms of surfactant availability and droplet size reduction capacity does not fully coincide with observations made with regard to stability under storage. It might have been expected that systems generated within the surfactant-poor regime would also exhibit poor emulsion stability, while those formed under a surfactant-rich environment would display long-term stability. Although this is indeed the case for the majority of the systems, there are outliers to this behavior. The 40 wt % oil mass content emulsion with a 0.1 wt % Tween20 concentration was previously suggested to arise from CIJM processing within the surfactant-rich regime; however, the long-term stability of this system is shown here to be compromised. Conversely, even though the 80 wt % oil mass fraction emulsions with either 1 or 2 wt % Tween20 concentrations were proposed to be formed within a surfactant-poor regime, both systems remained stable over the tested storage period. The link between surfactant availability during emulsion formation and consequent long-term stability is therefore much more complex. This equally implies that the surfactant-rich and surfactant-poor regimes are not always able to be clearly defined as well as that emulsion stability (even when the microstructure was originally formed under conditions of high availability of the interface stabilizing species) can be compromised by other factors, for example, changes to the conformation of the stabilizing species following their adsorption at an interface.[39]

4. CONCLUSIONS

This study first aims to assess the CIJM capacity to realize optimal processing environment under the hydrodynamic/formulation conditions investigated here, from both a computational and experimental perspective. It is suggested that optimal CIJM operation is realized when (i) the inlet jet mass flow rate, W_{jet}, > 176 g/min and at the same time (ii) the pre-emulsion $d_{3,2}$ is higher than the d_{max} evaluated under fixed W_{jet}.

DOI: 10.1021/acs.iecr.9b00634
Ind. Eng. Chem. Res. 2019, 58, 14859−14872

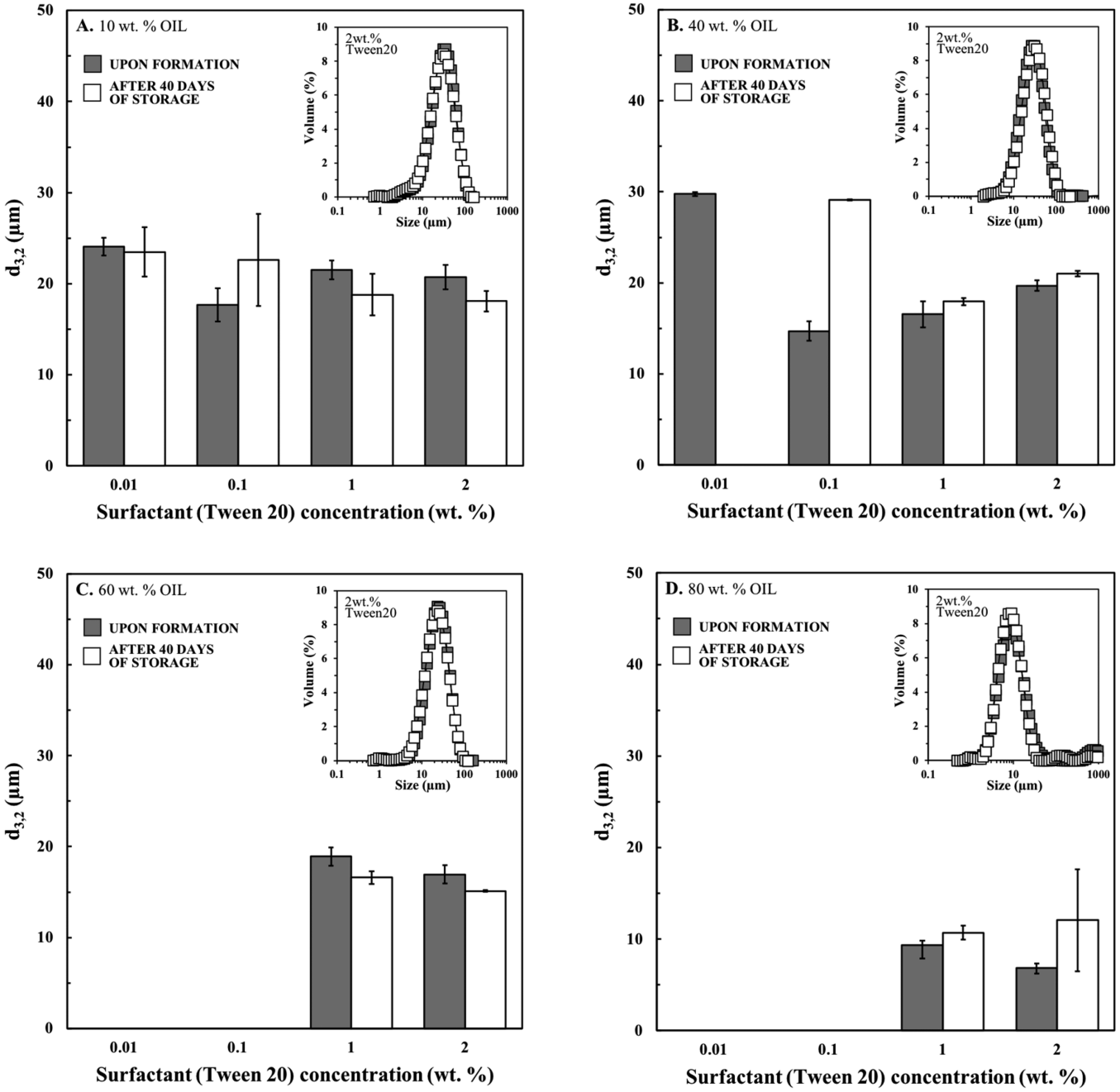

Figure 11. Long-term stability of emulsions with 10 (A), 40 (B), 60 (C), and 80 wt % (D) produced in the CIJM geometry (at a fixed jet mass flow rate of 352.75 g/min) as a function of surfactant (Tween20) concentration; solid (gray) and open bars represent Sauter mean diameters ($d_{3,2}$) immediately after CIJM processing and following a storage period of 40 d at room temperature (22 °C), respectively. All data points are mean values ($n = 2$), and error bars represent one standard deviation of the mean. (inset graphs) The droplet size distribution of each system (for a corresponding dispersed-phase fraction) stabilized by 2 wt % of Tween20, immediately after CIJM processing (solid gray symbols) and following a storage period of 40 d at room temperature, that is, 22 °C (open symbols).

After the findings of the first result section, the second part of this study focuses on the experimental assessment of the CIJM emulsification performance for the processing of o/w emulsions with a wide range of oil contents, in the surfactant-poor and surfactant-rich regimes, at different operational conditions and residence times. Overall, the pre-emulsion $d_{3,2}$ decreases as W_{jet} increases (within the optimal range of operation) independently on the dispersed-phase mass fraction. Under the strongest hydrodynamic conditions, all systems showed a similar droplet size distribution and polydispersity. It was also observed, on the basis of a comparison with the theoretically calculated Kolmogorov eddy size, a transition from a TI to TV regime of emulsification took place by increasing the oil mass fraction from 40 to 60 wt %. It is suggested as the emulsion droplet size reduction for highly concentrated systems (80 wt %) is instead due to the predominant hydrodynamic interactions between neighboring droplets rather than to turbulence effects. The increase of the residence time (e.g., multipassing) under fixed hydrodynamic conditions primarily causes a reduction of the span of the droplet size distribution of the processed emulsions.

It is also proposed that the ability of CIJM processing to reduce the emulsion $d_{3,2}$ is strongly dependent on the surfactant

DOI: 10.1021/acs.iecr.9b00634
Ind. Eng. Chem. Res. 2019, 58, 14859−14872

availability (e.g., surfactant concentration to the oil content). The $d_{3,2}$ of formulations with low surfactant availability (e.g., surfactant-poor regime) is majorly driven by surfactant concentration and oil content (e.g., formulation aspects) rather than the energy dissipation rate generated by jet collisions (e.g., processing aspects) as in the case of formulations with high surfactant availability (e.g., surfactant-rich regime).

Although most of the systems overall show a good stability upon storage regardless of their formulation, to establish a clear correlation between the surfactant availability and the long-term storage stability results in a rather complex operation.

In conclusion, this study offers novel insights into the emulsification by using CIJM, thus further extending the potential of its application for the (continuous, high-throughput, and low-energy) processing of more concentrated systems under a wide range of hydrodynamic conditions and formulation parameters.

■ ASSOCIATED CONTENT

Supporting Information

The Supporting Information is available free of charge on the ACS Publications website at DOI: 10.1021/acs.iecr.9b00634.

DSDs of 10 wt % o/w pre-emulsions after their preparation in the high-shear mixer (at 2000, 4000, 6000, and 9000 rpm) and following their processing in the CIJM cavity under the highest mass jet flow rate (702 g/min). Analogous trends were also observed for the DSDs of 40 wt % (pre-) emulsions (not shown), in the presence of 1 wt % of Tween20. Variation in DSD of pre-emulsions with increasing oil content (from 10 to 80 wt %) following their exposure to the highest mass jet flow rate (702 g/min), in the presence of 1 wt % of Tween20. DSDs of the final (10 to 80 wt %) o/w emulsions produced following one and after four passes through the CIJM geometry under fixed mass jet flow rate (352.75 g/min) and in the presence of 1 wt % of Tween20 (PDF)

■ AUTHOR INFORMATION

Corresponding Author

*Phone: +44 (0) 7521720608. E-mail: ext520@bham.ac.uk.

ORCID

Ernesto Tripodi: 0000-0001-8308-9925

Fotis Spyropoulos: 0000-0002-0872-9328

Author Contributions

The manuscript was written through contributions of all authors. All authors have given approval to the final version of the manuscript.

Notes

The authors declare no competing financial interest.

■ ACKNOWLEDGMENTS

This research was funded by the Centre for Innovative Manufacturing in Food and the Engineering and Physical Sciences Research Council (EP/K030957/1).

■ ABBREVIATIONS

CIJM = Confined Impinging Jet Mixers

TI = turbulent inertial

TV = turbulent viscous

■ REFERENCES

(1) Donsì, F. Applications of nanoemulsions in foods. In *Nanoemulsions;* McClements, D. J., Jafari, S. M., Eds.; Academic Press: London, UK, 2018; pp 349−377.

(2) Rayner, M. Scales and forces in emulsification. In *Engineering aspects of food emulsification and homogenization*; Rayner, M., Dejmek, P., Eds.; CRC Press: Boca Raton, FL, 2015, 3−32.

(3) Kolmogorov, A. N. Drop breakage in turbulent flow. *C. R. Acad. Sci.* **1949**, *66*.

(4) Hinze, J. O. Fundamentals of the hydrodynamic mechanism of splitting in dispersion processes. *AIChE J.*. **1955**, *1*.289

(5) Tcholakova, S.; Lesov, I.; Golemanov, K.; Denkov, N. D.; Judat, S.; Engel, R.; Danner, T. Efficient emulsification of viscous oils at high drop volume fraction. *Langmuir* **2011**, *27*, 14783.

(6) Vankova, N.; Tcholakova, S.; Denkov, N. D.; Ivanov, I. B.; Vulchev, V. D.; Danner, T. Emulsification in turbulent flow: 1. Mean and maximum drop diameters in inertial and viscous regimes. *J. Colloid Interface Sci.* **2007**, *312*, 363.

(7) Li, Z.; Dai, L.; Wang, D.; Mao, L.; Gao, Y. Stabilization and rheology of concentrated emulsions using the natural emulsifiers quillaja saponins and rhamnolipids. *J. Agric. Food Chem.* **2018**, *66*, 3922.

(8) Håkansson, A. In *Engineering aspects of food emulsification and homogenization;* Rayner, M.; Dejmek, P.; CRC Press: Boca Raton, FL, 2015; pp 125−148.

(9) Seekkuarachchi, I. N.; Tanaka, K.; Kumazawa, H. Formation and charaterization of submicrometer Oil-in-Water (O/W) emulsions, using high-energy emulsification. *Ind. Eng. Chem. Res.* **2006**, *45*. DOI: 10.1021/ie050323+

(10) Joscelyne, S. M.; Trägårdh, G. Membrane emulsification — a literature review. *J. Membr. Sci.* **2000**, *169*, 107.

(11) Lloyd, D. M.; Norton, I. T.; Spyropoulos, F. Processing effects during rotating membrane emulsification. *J. Membr. Sci.* **2014**, *466*, 8.

(12) Neethirajan, S.; Kobayashi, I.; Nakajima, M.; Wu, D.; Nandagopal, S.; Lin, F. Microfluidics for food, agriculture and biosystems industries. *Lab Chip* **2011**, *11*, 1574.

(13) McClements, D. J. *Food Emulsions: Principles, Practices and Techniques;* CRC Press: Boca Raton, FL, 2016.

(14) Johnson, B. K.; Prud'homme, R. K. Chemical processing and micromixing in confined impinging jets. *AIChE J.* **2003**, *49*, 2264.

(15) Siddiqui, S. W.; Zhao, Y.; Kukukova, A.; Kresta, S. M. Characteristics of a Confined Impinging Jet Reactor: energy dissipation, homogeneous and heterogeneous reaction products, and effect of unequal flow. *Ind. Eng. Chem. Res.* **2009**, *48*, 7945.

(16) Liu, Y.; Fox, R. O. CFD predictions for chemical processing in a confined impinging-jets reactor. *AIChE J.*. **2006**, *52*. DOI: 10.1002/aic.10633

(17) Gavi, E.; Marchisio, D. L.; Barresi, A. A. CFD modelling and scale-up of Confined Impinging Jet Reactors. *Chem. Eng. Sci.* **2007**, *62*, 2228.

(18) Siddiqui, S. W. Mixing performance of various geometries - Emulsification perspective. *Procedia Food Sci.* **2011**, *1*, 131.

(19) Siddiqui, S. W.; Norton, I. T. Oil-in-water emulsification using Confined Impinging Jets. *J. Colloid Interface Sci.* **2012**, *377*, 213.

(20) Siddiqui, S. W.; Wan Mohamad, W. A. F.; Mohd Rozi, M. F.; Norton, I. T. Continuous, high-throughput flash-synthesis of submicron food emulsions using a Confined Impinging Jet Mixer: effect of in situ turbulence, sonication, and small surfactants. *Ind. Eng. Chem. Res.* **2017**, *56*, 12833.

(21) Barnes, H.; Hutton, J. F.; Walers, K. *An introduction to Rheology;* Elsevier: Amsterdam, Netherlands, 1989.

(22) Calabrese, R. V.; Wang, C. Y.; Bryner, N. P. Drop breakup in turbulent stirred-tank contactors. Part III: Correlations for mean size and drop size distribution. *AIChE J.* **1986**, *32*, 677.

(23) Siddiqui, S. W. The effect of oils, low molecular weight emulsifiers and hydrodynamics on oil-in-water emulsification in Confined Impinging Jet Mixer. *Colloids Surf., A* **2014**, *443*, 8.

(24) Sprow, F. B. Distribution of drop sizes produced in turbulent liquid—liquid dispersion. *Chem. Eng. Sci.* **1967**, *22*, 435.

(25) Zhou, G.; Kresta, S. M. Correlation of mean drop size and minimum drop size with the turbulence energy dissipation and the flow in an agitated tank. *Chem. Eng. Sci.* **1998**, *53*, 2063.
(26) Pacek, A. W.; Man, C. C.; Nienow, A. W. On the Sauter mean diameter and size distributions in turbulent liquid/liquid dispersions in a stirred vessel. *Chem. Eng. Sci.* **1998**, *53*, 2005.
(27) Jafari, S. M.; Assadpoor, E.; He, Y.; Bhandari, B. Re-coalescence of emulsion droplets during high-energy emulsification. *Food Hydrocolloids* **2008**, *22*, 1191.
(28) Tesch, S.; Gerhards, C.; Schubert, H. Stabilization of emulsions by OSA starches. *J. Food Eng.* **2002**, *54*, 167.
(29) Floury, J.; Desrumaux, A.; Lardières, J. Effect of high-pressure homogenization on droplet size distributions and rheological properties of model oil-in-water emulsions. *Innovative Food Sci. Emerging Technol.* **2000**, *1*, 127.
(30) Narsimhan, G.; Goel, P. Drop coalescence during emulsion formation in a High-Pressure Homogenizer for tetradecane-in-water emulsion stabilized by sodium dodecyl sulfate. *J. Colloid Interface Sci.* **2001**, *238*, 420.
(31) Golemanov, K.; Tcholakova, S.; Denkov, N. D.; Ananthapadmanabhan, K. P.; Lips, A. Breakup of bubbles and drops in steadily sheared foams and concentrated emulsions. *Phys. Rev. E* **2008**, *78*, 78.
(32) Walstra, P., 8 - Emulsions. In *Fundamentals of Interface and Colloid Science*; Lyklema, J.; Academic Press: London, UK, 2005; pp 8.1−8.94.
(33) Lee, L.; Norton, I. T. Comparing droplet breakup for a high-pressure valve homogeniser and a Microfluidizer for the potential production of food-grade nanoemulsions. *J. Food Eng.* **2013**, *114*, 158.
(34) Qian, C.; McClements, D. J. Formation of nanoemulsions stabilized by model food-grade emulsifiers using high-pressure homogenization: Factors affecting particle size. *Food Hydrocolloids* **2011**, *25*, 1000.
(35) Tcholakova, S.; Denkov, N. D.; Danner, T. Role of surfactant type and concentration for the mean drop size during emulsification in turbulent flow. *Langmuir* **2004**, *20*, 7444.
(36) Taisne, L.; Walstra, P.; Cabane, B. Transfer of oil between oil droplets. *J. Colloid Interface Sci.* **1996**, *184*, 378.
(37) Lobo, L.; Svereika, A. Coalescence during emulsification: 2. Role of small molecule surfactants. *J. Colloid Interface Sci.* **2003**, *261*, 498.
(38) Tcholakova, S.; Denkov, N. D.; Lips, A. Comparison of solid particles, globular proteins and surfactants as emulsifiers. *Phys. Chem. Chem. Phys.* **2008**, *10*, 1608.
(39) Tcholakova, S.; Denkov, N. D.; Ivanov, I. B.; Campbell, B. Coalescence stability of emulsions containing globular milk proteins. *Adv. Colloid Interface Sci.* **2006**, *123*, 259.

DOI: 10.1021/acs.iecr.9b00634
Ind. Eng. Chem. Res. 2019, 58, 14859−14872